Novel thiol-grafted composite of chitosan and rice straw biochar (TH@CT-BC): A two-step fabrication for highly selective adsorption of cadmium from contaminated water

Yasir Hamid, Lei Liu, Muhammad Haris Mahyuddin, Muhammad Usman Hadi, Qiang Lin, Yonglong Chen, Muhammad Saqib Rashid, Zaid Ulhassan, M. Iftikhar Hussain, Xiaoe Yang

Novel thiol-grafted composite of chitosan and rice straw biochar (TH@CT-BC): A two-step fabrication for highly selective adsorption of cadmium from contaminated water

Yasir Hamid[1]*, Lei Liu[1], Muhammad Haris[2], Muhammad Usman[3], Qiang Lin[1], Yonglong Chen[1], Muhammad Saqib Rashid[4], Zaid Ulhassan[5], M. Iftikhar Hussain[6], Xiaoe Yang[1]*

[1]Ministry of Education (MOE) Key Lab of Environ. Remediation and Ecol. Health, College of Environmental and Resources Science, Zhejiang University, Hangzhou 310058, China

[2]School of Environmental Science and Engineering, Shaanxi University of Science & Technology, Xi'an 710021, PR China

[3] Université de Rennes, Ecole Nationale Supérieure de Chimie de Rennes, CNRS, ISCR-UMR 6226, F-35000, Rennes, France

[4]CAS-Key Laboratory of Crust-Mantle Materials and the Environments, School of Earth and Space Sciences, University of Science and Technology of China, Hefei 230026, P.R. China

[5]Institute of Crop Science, Ministry of Agriculture and Rural Affairs Laboratory of Spectroscopy Sensing, Zhejiang University, Hangzhou 310058, China

[6]Department of Plant Biology & Soil Science, Universidade de Vigo, Campus Lagoas Marcosende, 36310-Vigo, Spain

* For correspondence:

xeyang@zju.edu.cn (X. E Yang), yasirses2007@gmail.com (Y. Hamid)

Abstract

This study followed the one-step and two-step technologies to produce rice straw biochar (BC), chitosan-modified rice straw biochar (CT-BC), and thiol grafted chitosan-modified biochar (TH@CT-BC) for cadmium (Cd) removal from contaminated water. Here, chitosan and thiol were introduced by two-step combination to enhance the adsorption ability of biochar. Our results revealed the maximum Cd adsorption at pH 5.5 with TH@CT-BC (261.47 mg g^{-1}) followed by CT-BC (103.14 mg g^{-1}) and BC (29.64 mg g^{-1}). Obtained data was best fitted by the Langmuir and pseudo-second-order kinetic models (with R^2 values of 0.997 for TH@CT-BC) as compared to Freundlich and Temkin models (0.949 and 0.925, respectively). TH@CT-BC retained its efficiency in spiked river water system, removing up to 89% of Cd in river water spiked with 30 mg^{-1} L Cd. The experimental investigations and data calculations demonstrated the surface complexation and electrostatic interaction as dominant underlying mechanisms for Cd removal by TH@CT-BC. Moreover, it is essential to utilize the large amount of produced rice straw to develop new materials which would help in converting the waste to useable product for environmental remediation. Thus, this study demonstrates the production of TH@CT-BC from rice straw as an effective adsorbent of Cd from aqueous systems which can be studied as a potential candidate for practical wastewater treatment applications.

Keywords: Rice straw biochar; Chitosan; Thiol modification; Cadmium; Adsorption; River Water

1. Introduction

Recently, biochar (BC) has found numerous applications for soil remediation, water treatment, energy storage, carbon sequestration, and crop yield improvement (Qi et al., 2017; Xia W et al., 2022). Advances in biochar technology have satisfied the need of a cost-effective treatment for aqueous environment. For instance, Chen et al. (2011) effectively removed copper and zinc using wood and corn-derived biochar. Similarly, oak bark biochar was more effective in removing cadmium (Cd) as compared to commercially available activated carbon (Mohan et al., 2007). However, pristine biochar often exhibits limited potential in water treatment due to its poor selectivity, lower adsorption capacity, and regeneration inefficiency (Mohan et al, 2014; Inyang et al., 2016). These limitations can be addressed by modifying or functionalizing the pristine BC into advanced materials having improved physico-chemical properties and extended environmental applications spectrum (Krasucka et al., 2021; Hamid et al., 2022; Wang et al., 2023).

Present study focuses on the synthesis and application of thiol grafted chitosan-modified rice straw biochar (TH@CT-BC) for Cd removal from contaminated water. Chitosan (CT), a natural polysaccharide, easily obtained from chitin is the second most prevalent polymer after cellulose (Abd Malek et al., 2021). It is a biocompatible, non-toxic, and renewable material (Turan, 2019). Moreover, free hydroxyl and amino groups of CT along with its high abundance, low cost, biocompatibility, biodegradability, nontoxicity, and adsorption capacity make it a viable adsorbent for the removal of heavy metals (Zhou et al., 2013; Zhang et al., 2019). However, high solubility of CT powder, poor stability and reusability, low surface area, and limited number of active sites can restricts its applications for industrial wastewater treatment (Jawad et al., 2021).

It is worthy to note that surface modification of BC is usually achieved by introducing/loading of functional groups/materials, generally through chemical co-precipitation (Ahmed et al., 2016). However, the co-precipitated compounds may tend to agglomerate or detach after a certain period (Jawad et al., 2021). To address this, further modification of BC surface with thiol (TH) group (–SH) can lead to the stable complexation of heavy metals onto BC surface (Xia et al., 2019). Thiol modification is a well-established method to enhance the functional properties and adsorption capacity of carbon materials. Moreover, TH group demonstrates stronger bonding ability towards heavy metals than halogen atoms, oxygenic functional groups, and amino groups (Kazemi et al., 2016). Meanwhile, the presence of TH group can induce high selectivity for the removal of specific pollutants in co-contaminated surface/ground water (Chai et al., 2010; Jiang et al., 2016).

Cadmium, a toxic heavy metal, is commonly found in industrial effluents, mining wastewater, and agricultural runoff. It is considered a model pollutant due to its high toxicity and prevalence in various industrial processes (Ma et al., 2018). In adsorption experiments, Cd is often used as a representative pollutant to evaluate the efficacy of adsorbent materials in removing heavy metals from contaminated waters. The use of Cd as a model pollutant in adsorption experiments provides valuable insights into the effectiveness of different adsorbent materials for real-world application (Hamid et al., 2022).

The development of highly efficient, stable, cost-effective, and environment-friendly adsorbents is an on-going research hotspot to enhance their practical applications (Jawad et al., 2022). Here, we present a two-step fabrication strategy to develop a highly proficient, chemically stable, and effective adsorbent. The surface modification of BC was achieved with CT coating by mechanical mixing to produce CT-BC composite (1). To overcome the above discussed limitations of pristine BC and CT, CT-BC was further modified with TH using 3- MPTS to produce TH@CT-BC

composite having extra SH-groups on the BC surface. Later, pristine and modified BCs were studied for Cd removal from contaminated water. The specific objectives of our study were (a) to synthesize and characterize the pristine and modified BC (BC, CT-BC, and TH@CT-BC) by revealing the structural/surface and physicochemical properties; (b) to evaluate the adsorption kinetics and adsorption capacity of BC, CT-BC, and TH@CT-BC for Cd; (c) to unravel the possible adsorption mechanisms of Cd; and (d) to study the effectiveness of two-step technology in Cd removal from river water. We anticipate that the results of this study may provide important insights into the highly effective adsorption of pollutants using a novel adsorbent for wastewater treatment and industrial application.

2. Materials and methods

2.1. Materials

All the chemicals used in this study were of analytical or higher grade. $CdCl_2$ was obtained from Shanghai Aladdin Biochemicals while, $K_2Cr_2O_7$, HCl, CH_3COOH, $CaCl_2$, and HNO_3 were acquired from Sinopharm Chemical Reagent Co., Ltd (Shanghai, China). Chitosan was supplied by Sinopharm Chemical Reagent Co., Ltd (Shanghai, China). Ethanol and 3-mercaptopropyltrimethoxysilane (3- MPTS 97%) was procured from J&K Scientific (Beijing, China). Analytical grade NH_4OH was supplied by Tianjin Chemical Reagent Technology (Tianjin, China). All experimental solutions were prepared using ultrapure water exhibiting high resistivity (18.2 MΩ.cm at 25 °C).

2.2. Preparation of pristine biochar (BC), chitosan-modified biochar (CT-BC), and thiol grafted-chitosan-modified biochar (TH@CT-BC)

Pristine BC was produced from rice straw, a common agricultural waste collected from the nearby field in Hangzhou, China. The collected biomass material was air-dried, chopped into small pieces, and pyrolyzed under N_2-flow conditions for 2 h at 500 ^oC. The resulting BC was then crushed and sieved (0.5-1 mm) for a uniform size fraction before being stored for further use. The resulting as-is BC sample from rice straw is referred as BC.

Analytical grade CT (100,000–300,000 g mol^{-1} viscosity molecular weight) was used to modify the BC. In brief, CT (3 g) was firstly dissolved in 180 mL of 2% acetic acid. Subsequently, 3 g of BC was added to the solution and continuously stirred for 30 min. Then, the homogeneous mixture of CT-BC was added drop wise in 900 mL of 1.2% NaOH solution and kept in the solution for 12 h. The excess NaOH was removed by washing the CT-modified BC with deionized water (UP water) and oven dried for 24 h at 70 $^{\circ}C$. The resulting CT-modified BC is referred as CT-BC.

The thiol grafted-chitosan-modified BC was prepared by a modified ammonium hydroxide method (He et al. 2012; Huang et al., 2017). Briefly, CT-BC (6 g) was transferred into a glass beaker (250 mL) containing water (7.2 mL) and ethanol (228 mL). 3-MPTS (4.8 mL) was poured drop wise with continuous stirring magnetically under nitrogen protection. After 6 h of magnetic stirring, the pH of the solution was adjusted to 9.5 with NH_4OH and reaction time was exceeded to 24 h. As a final point, the particles were washed with ethanol and deionized water three times in turns. The final product was then freeze-dried under vacuum for 48 h and the thiol grafted-chitosan-modified biochar was named as TH@CT-BC.

2.3. Characterization of biochars

The surface morphology and structural differences of BC, CT-BC, and TH@CT-BC were characterized using scanning electron microscopy (SEM) (Gemini SEM 300). Fourier

transform infrared (FTIR) spectra were taken through a Nicolet 6700 spectrometer with 50 scans at 2 cm^{-1} in a range of 400–4000 cm^{-1}. The surface elements of the simple and functionalized material were analyzed by using energy dispersive X-ray spectroscopy (EDS). The binding energies and surface atomic ratios were analyzed by X-ray photoelectron spectroscopy (XPS). The X-ray diffractometer (XRD) explored the crystal structure by taking scans from 5° to 80° (2θ). C, H, and N contents were examined by elemental analyzer (varioMICRO CHN) while, pH of the pristine and functional BCs was measured using a pH meter (PB-10, Sartorius, Germany).

2.4. Batch adsorption experiments

The effectiveness of pristine and modified BCs was investigated under different batch adsorption tryouts. The stock solution of Cd (1000 mg/L) was prepared from $CdCl_2$ and solution pH was adjusted (pH=5.5 ± 0.5) by adding HNO_3 or NaOH. The kinetic study was done by adding a defined amount of BC, CT-BC, and TH@CT-BC (0.05 g) into different PTFE tubes containing 35 mL of Cd(II) solution. The tubes were then stirred for 24 h at 200 rpm at an average temperature of 26 ± 2 ºC. The samples were collected at specific time intervals (5, 10, 20, 30, 60, 120, 240, 480, 960, and 1440 min), centrifuged for 15 min, and the suspension was passed through membrane filters (0.22 µm). After filtration, the insulated samples were acidified with 1% HNO_3 and subjected to inductively coupled plasma mass spectrometry (ICP-MS, Agilent, 7500a, USA) for the determination of metal concentration. The final concentration of the adsorbed Cd onto the adsorbent at certain time and percentage removal/adsorption percentage were calculated using the following formulas

$$qe = \frac{(Co - Ce)V}{m} \qquad 1$$

$$R\% = \frac{(Co-Ce)}{Co} * 100 \qquad 2$$

Here, qe and R% denotes adsorption capacity and removal percentage/adsorption percentage, respectively. While, Co depicts the initial concentration and Ce is the equilibrium metal concentration, m (g) is mass of the adsorbent, and V (L) is the volume of the solution containing metal.

2.4.1 Effect of pH

The effect of solution pH on Cd adsorption was investigated by adjusting the initial pH of the solution (30 mg L^{-1} Cd) from 1 to 10 using HCl and/or NaOH. The residual Cd concentration in solution after adsorption was calculated as discussed above in section 2.6.

2.4.2 The equilibrium study

Equilibrium experiments were performed to assess the adsorption capacity of BC, CT-BC, and TH@CT-BC by loading a fixed amount of adsorbent (0.05 g) into 35 mL of metal solution (pH=5.5 ± 0.5) with initial concentrations of 10, 30, 60, 90, and 150 mg L^{-1}. The adsorption equilibrium was achieved by shaking the flasks at 200 rpm for 24 h at 26 ± 2 ^{o}C. The samples were then centrifuged, filtered, and metal content was measured using ICP-MS.

The equilibrium adsorption isotherms including Langmuir, Freundlich, and Temkin isotherms were used to fit the experimental data. The Langmuir isotherm describes the homogenous adsorption over the sorbent while; Freundlich isotherm defines the chemisorption process.

Langmuir equation: $$q_e = \frac{q_m \cdot K_L \cdot C_e}{1+K_L \cdot C_e} \qquad 3$$

Freundlich model: $q_e = K_F \cdot C_e^{\frac{1}{n}}$ 4

Temkin equation: $q_e = \left(\frac{RT}{b}\right) \ln(AC_e)$ 5

Here, q_e denotes adsorbed Cd at equilibrium, q_m presents maximum capacity of Cd uptake (mg g^{-1}), K_L (L/mg) is equilibrium constant, and C_e (mg L^{-1}) is the Cd concentration at equilibrium and K_F, K_L, and A are Freundlich, Langmuir, and Temkin isotherm constant (L g^{-1}). Moreover, n presents the heterogeneity factor while T is absolute temperature (K) and R represents general gas constant (8.314 $\times 10^{-3}$ KJ mol^{-1} K^{-1}).

The kinetic data was analyzed by non-linearized equations of pseudo-first-order (6), pseudo-second-order (7), and intraparticle diffusion (8) equations as presented follows

$$q_t = q_e\left(1 - e^{(-k_1 t)}\right) \quad 6$$

$$q_t = \frac{k_2 q_e^2 t}{1 + k_2 q_e t} \quad 7$$

$$q_t = k_p t^{1/2} + C \quad 8$$

here q_e is the amount of metal adsorbed (mg g^{-1}) at equilibrium time, q_t is the amount of metal adsorbed at time t (min), and k_1 (1 min^{-1}) , k_2 (g mg^{-1} min^{-1}), k_p stands for intraparticle diffusion rate constant and C indicates the boundary layer effect (mg g^{-1}) and was calculated from the plot q_t vs $t^{0.5}$.

2.4.3 Adsorption selectivity experiment

The selective adsorption of Cd onto BC, CT-BC, and TH@CT-BC was studied by deploying 0.05 g of adsorbents into a mixture containing different concentrations (0.1, 0.5, and 1.0 mmol/L) of Cd, Pb, Zn, Mg, Cu, and Ni. The mixture (pH=5.5 ± 0.5) was stirred for 24 h at 200 rpm at 26 ± 2

^{o}C. The samples were filtered (0.22 µm membrane filters) and Cd concentration in the metal solution was determined using ICP-MS.

2.4.4 Regeneration study

The regeneration and recycling experiments were performed by agitating 0.05 g of tested adsorbents in a Cd solution (30 mg L^{-1}) for 4 h at 200 rpm and 26 ± 2 ^{o}C (pH=5.5 ± 0.5). The solution was probed to ICP-MS to determine the metal concentration. Moreover, desorption of Cd with applied treatments was investigated by using desorption agents including HCl or HNO_3. In brief, 2 mL of HCl or HNO_3 was mixed with the collected adsorbent from the adsorption experiment and shaken for 1 h at 200 rpm to remove the adsorbed Cd onto pristine or modified BC. The collected adsorbent was washed with distilled water, dried, and used in next desorption cycle with a minimum of five adsorption/desorption cycles. The remaining metal content in each cycle was determined using ICP-MS.

2.4.5 Spiked river water study

The spiked river water study was employed to assess the efficacy of BC, CT-BC, and TH@CT-BC by using the filtered river water collected from Zhixi river (pH 7.59), artificially spiked with Cd (10 and 30 mg L^{-1}) to imitate the real application situation. A distinct amount of adsorbent was loaded into 35 mL of metal containing river water, agitated at 200 rpm for 24 h at 26 ± 2 ^{o}C. The samples were filtered and Cd content in filtrate was analyzed using ICP-MS.

2.5. Data analysis and quality control

The pristine and modified BCs were synthesized and characterized in controlled temperature conditions in lab. The adsorption tests for Cd were conducted in triplicate for each treatment.

Moreover, appropriate blanks of Cd solution without the use of adsorbents were employed to evaluate any metal loss during sorption trials. The recovery of samples remained between 90-110% and blank data were below the detection limits. The data fitting for kinetics and isotherm models was evaluated with R^2 value where higher value indicates the better curve fitting.

3. Results and discussion

3.1. Characterization of pristine and modified biochars

The pristine BC was characterized by higher concentration of C (49.64%), H (2.26%), and N (1.23%). However, modification of BC with CT and TH decreased the C contents to 38.35 and 33.67% for CT-BC and TH@CT-BC, respectively, while the H contents were increased to 3.97 and 4.90%, respectively. However, CT modification increased the N contents (2.27%), whereas TH modification decreased the N contents to 0.75%. The C/N ratio of BC, CT-BC, and TH@CT-BC used in this study was 40, 17, and 44, highlighting the role of CT in lowering the C/N ratio only in CT-BC. Meanwhile, BC displayed a higher specific surface area (12.36 m^2/g) which decreased after modification with CT and TH (4.87 and 3.59 m^2/g), respectively (Table 1). This decrease in surface area might be attributed to the occlusion of pore openings or partial infilling of pores during modification (Zhou et al., 2013).

The morphological differences between BC, CT-BC, and TH@CT-BC were examined through SEM and EDS spectroscopy (Figure 1). The SEM images of BC revealed irregular and porous structure but CT-BC and TH@CT-BC presented honey-comb structures with relatively shredded pores, revealing nano-sheets of modified materials. Moreover, the EDS analysis of BC depicted the abundance of C, O, Si, K, and P (80.69, 12.95, 2.62, 1.79, and 0.64%), respectively as dominant elements. The modification of BC with CT (CT-BC) resulted in a reduction in C contents while

increased the O and P in the modified BC. The elemental composition of CT-BC was revealed as C (50.74%), O (38.35%), Si (6.45%), K (1.63%), and P (1.25%). Similarly, TH modification (TH@CT-BC) decreased the C content while increasing the O concentration. The overall elemental composition trend was observed as C > O > Si > S > P (45.24, 30.83, 12.38, 10.99, and 1.097%). Here, the higher contents of Si and the introduction of S might be linked to the TH modification, as described in previous studies (Huang et al., 2019a).

The FTIR analysis revealed an increase in the type and abundance of functional groups after modification (Figure 1). The broad adsorption peak for BC at ~3406 cm^{-1} was attributed to the presence of O–H group. The bands at ~1590 and 1412 cm^{-1} were assigned to the C─O and benzene ring which belongs to the lignin in rice straw (Xu et al., 2022). FTIR spectra of CT-BC and TH@CT-BC exhibited abundant O─H and N─H stretching vibrations at ~3000 and 3700 cm^{-1}. Peaks at ~1000, 1100, and 1200 cm^{-1} might be ascribed to the presence of C─OH vibrations. Similarly, TH modification increased the active oxygenic functional groups e.g. ─OH, C─O─C, and C═O and π bond onto BC surface which might serve as the active sites for the binding of pollutants to 3-MPTS (Tang et al., 2016: Huang et al., 2019b). Pristine and modified BCs had alkaline pH with more oxygenic functional group in BC, which were further occupied by 3-MPTS during the TH modification.

The XRD patterns of pristine and modified BCs are presented in (Figure 1). The XRD analysis of BC depicted the abundance of inorganic minerals including SiO_2, KCl, and $CaCO_3$ at $2\theta=26.62^o$, 40.50^o, and 50.58^o, respectively (Sackey et al. 2021). Notably, CT-BC showed a number of new reflections depicting the formation of crystalline structures (SiO_2 and $CaCO_3$). Here diffraction peaks of SiO_2 showed the dispersion of pristine BC in the composite. The diffraction peaks around $2\theta=16^o$ and 20^o might be allocated to the presence of crystalline structures of CT. However, the

XRD pattern of TH@CT-BC did not show any obvious diffraction peaks and depicted an amorphous structure, where peak around 21.1^{o} indicated the presence of a certain amount of silane molecules (Xiao et al. 2013). The loss of hydroxyl and amino groups due to the introduction of TH groups could have contributed to this disappearance of peaks after TH modification (Xia et al., 2019).

High resolution XPS analysis of O1s, C1s, and N1s depicted the chemical composition of pristine and modified BCs and are presented in Figure 2 (TH@CT-BC) and Figure S1 (BC and CT-BC). The O1s peaks at 530.84, 531.69, and 532.79 eV corresponds to the (O–H), (C=O), and (C–O), respectively (Zhang, L et al., 2019). The peaks at 532.79 eV correspond to the carbonyl group (C=O). Similarly, the C1s spectrum exhibited the peaks at 284.05, 284.67, and 285.6 eV which were attributed to C=C/C–C, C–O, respectively. Moreover, peaks corresponding to 286.17, 287.9, and 288.04 eV portrays the presence of C–OH, C=O, and C=O/O–C=O, respectively showing the abundance of oxygenic moieties after modifications. On the other hand, the wide scans of XPS displayed new peaks N1s for BC, CT-BC, and TH@CT-BC. The modified BCs indicated the existence of C=N, –NH–, and $–NH_2$/$–NH_3^+$ as evident from the appearance of the associated peaks at 398.59, 399.36, and 400.38 eV where ($–NH_2$/$–NH_3^+$) was specifically found in CT-BC and TH@CT-BC. Moreover, oxygenic moieties were considerably improved after the modification. The BC presents 15.54% oxygenic content which was elevated to 26.42 and 32.84% in CT-BC and TH@CT-BC, respectively, implying that modification of BC was helpful in increasing the surface functional moieties.

3.2. Sorption kinetic and isotherms

Dynamics of the mass transfer adsorption mechanisms and their rate-limiting factors can be determined through adsorption kinetic studies (Haris et al., 2022; Bahrudin et al., 2020). The kinetic adsorption of Cd onto BC, CT-BC, and TH@CT-BC was studied with an initial Cd concentration of 40 mg L^{-1}, adsorbent dosage 0.05 g, temperature 26±2 ^{o}C, and pH 5.5±0.5 (Figure 3A). It was observed that TH@CT-BC exhibited an L shape curve with two distinct phases. The first phase demonstrated fast adsorption, followed by the second phase of slower adsorption, ultimately reaching the equilibrium within 120 min, depicting the strong adsorption ability of TH@CT-BC towards Cd. This can be explained by the fact that most accessible adsorption sites were occupied first. On the other hand, CT-BC displayed lower adsorption efficiency (21.87 mg L^{-1}) followed by BC (11.82 mg L^{-1}), whereas it demonstrated a short adsorption equilibrium time as compared to TH@CT-BC and BC. The adsorption data was fitted with two major kinetic models including pseudo-first-order and pseudo-second-order (Table S1). Pseudo-first-order is based on the membrane diffusion theory, suggesting that the adsorption rate is linked with the adsorption uptake and equilibrium adsorption uptake. However, pseudo-second-order is established on the rate-limiting factor of adsorption (Huang et al., 2019a). For all the adsorbents, adsorption data best fit the pseudo-second-order yielding corresponding R^2 values of 0.992, 0.990, and 0.997 for BC, CT-BC, and TH@CT-BC, respectively. The results of the kinetic study further explain chemisorption as the rate-limiting factor which occurs due to the sharing/exchange of electrons between the adsorbate and adsorbent (Liu et al., 2019). The adsorption equilibrium can be evaluated by the k-constant which signifies the impact of time-scaling factor in achieving the quick adsorption equilibrium (Zhang, Y et al., 2019). The sorption rate was assessed with the k values which imply that CT-BC had a higher k value (0.062) than TH@CT-BC and BC (0.009 and 0.0014, respectively) indicating that TH@CT-BC required less time to achieve equilibrium than BC. It

was worthy to note that the first steep slope presents the instantaneous adsorption of Cd onto the surface of modified BC which might be linked to the electrostatic interaction, while second gentle slope is dominated by precipitation or complexation mechanisms. Hence, it can be concluded that adsorption kinetics mainly embraces three steps including internal diffusion, external diffusion, and adsorption on binding sites (Xie et al., 2019). Thus, kinetic results were further fitted with the intraparticle diffusion model to gain insights into the adsorption mechanisms and rate-limiting factors. The linear nature of graphs developed by intraparticle diffusion model describes the involvement of internal diffusion as a rate-limiting factor in sorption mechanisms. In our study, the graphs of Qt vs $t^{0.5}$ for Cd adsorption depicted three discrete slopes (Figure 3B) implying the involvement of three main stages in adsorption including external diffusion of Cd onto adsorbent, internal diffusion, and equilibrium stage (Wang et al., 2010). The intraparticle diffusion constant (k_p) for BC, CT-BC, and TH@CT-BC decreased in the following order: kp1 > kp2 > kp3 with values (1.55, 0.12, 0.045; 2.65, 0.14, 0.051; 5.57, 0.13, 0.036), respectively (Table S2). These results indicate the direct correlation between internal diffusion and Cd adsorption onto the tested materials (Xue et al., 2012). Moreover, higher values of k_p for CT-BC and TH@CT-BC indicate the faster adsorption of Cd which aligns with the results of the pseudo-second-order model.

The adsorption isotherm points the interfaces between the amount of Cd adsorbed by the applied additives and concentration of Cd in the solution after achieving equilibrium. For the adsorption isotherms, Freundlich, Langmuir, and Temkin models were employed to fit the sorption data of Cd by BC, CT-BC, and TH@CT-BC (Figure 4) and calculations of the fitted parameters are presented in Table 2. The Langmuir isotherm model demonstrated the highest correlation coefficients (R^2, for example 0.987 for TH@CT-BC) for Cd than those of the Freundlich and the Temkin models. The Langmuir model assert the monolayer sorption onto homogenous surface

(Langmuir, 1917), while the Freundlich model assumes the sorption onto heterogeneous surface (Freundlich, 1906). Moreover, the Temkin model reports the effect of certain adsorbate/adsorbate interactions on adsorption and illustrates a linear reduction in adsorption heat with coverage (Haris et al., 2022; Lima and Adebayo, 2015). Thus, Cd adsorption onto modified BCs can be pointed out as monolayer sorption. The deduced value of Q_{max} from Langmuir model depicts the actual adsorption capacity of BC, CT-BC, and TH@CT-BC for Cd with values 29.64, 103.14, and 261.47 mg g^{-1}, respectively. In our study, TH@CT-BC presented higher adsorption capacity, implying its potential for practical applications in treating contaminated water (Table 3).

3.3. Effect of solution pH on Cd adsorption

The solution pH is an important parameter in the adsorption process due to its influence in metals speciation and the surface charge of the adsorbent (Pehlivan et al., 2008). The adsorption of Cd on BC, CT-BC, and TH@CT-BC in response to changes in solution pH (from 1–10) is shown in Figure S2. Our results showed that TH@CT-BC presented highest adsorption capacity at pH around 5. Moreover, it retained the similar efficiency without any significant decline till pH 10 (Figure S2 in Supplementary Information). Furthermore, under low pH conditions, the TH@CT-BC composite likely to possess a positively charged surface, causing the surface functional groups to strongly interact with hydronium ions, which competes with the metals for sorption sites (Fan et al., 2013; Zhou et al., 2013). On the other hand, when solution pH is higher, the adsorption sites undergo deprotonation, leading to increased attraction between Cd ions and the surface functional groups, which facilitates the adsorption of Cd sorption onto modified BC (Wan et al., 2010; Huang, Y et al., 2019b).

3.4. Effect of competing cations

Typically, wastewater contains mixed pollution containing several metallic cations making the removal of the desired metal in co-existence with other pollutants very valuable. So, the uptake of Cd from a mixed solution of various metals (Ni, Zn, Pb, Mg, and Cu) at different concentrations (0.1, 0.5, and 1.0 mmol/L) was investigated through a batch adsorption experiment by deploying BC, CT-BC, and TH@CT-BC as adsorbents. As shown in Figure S3, Pb, Cu, and Ni exerted a greater impact on Cd adsorption, resulting in a decrease in Cd adsorption with an increase in concentration of competing metallic compounds. This can be linked to the difference in hydrated radius of metal cations. However, Zn and Mg did not pose a significant influence on Cd adsorption (81.06 and 79.11 mg g^{-1}) in 1.0 mmol/L solution. At a higher concentration of co-existing metals (1.0 mmol/L), TH@CT-BC retains more Cd as compared to BC and CT-BC. TH@CT-BC showed selective adsorption of Cd in the presence of co-existing metal cations (1.0 mmol/L) in the order of Ni > Zn > Pb > Mg > Cu displaying the concentration 82.54, 82.01, 81.18, 81.06, and 79.11 mg g^{-1}, respectively. Moreover, at an initial concentration of 1.0 mmol/L, CT-BC and BC showed the selective adsorption of Cd as compared to other cations as follows: Zn > Pb > Mg ≥ Cu > Ni and Mg > Zn > Cu > Pb > Ni, respectively. These results demonstrate the potential of TH@CT-BC for wastewater treatment in the presence of multiple cations.

It is well reported that metal ions with smaller hydrated radius had strong affinity for adsorption onto the adsorbents (Zhang et al., 2018) (Table S3). Among the cations, Pb had smaller hydrated radius which might help in selective adsorption of Pb onto the TH@CT-BC. However, low electronegativity and large hydrated radius of Mg reduced its affinity for TH@CT-BC. Therefore, metals with higher hydrated radius and lower electronegativity might have less affinity for hydroxyl, carboxyl, and amine groups (She et al., 2018). Moreover, TH@CT-BC contains numerous carboxyl and amine groups, which supported the higher selective adsorption of Cd onto

its surface (Zhou et al., 2013). Another precise explanation about the favorable adsorption of Cd might be related to the thiol group which works as soft Lewis base and have strong affinity for soft Lewis acids (e.g. Cd) (Deng et al., 2016). In a nut shell, the amount of Cd adsorption onto the adsorbent depends upon electronegativity of metals, hydrated radius, stability of metal hydroxides, and ionic potential (She et al., 2018; Wan et al., 2020).

3.5. Cadmium adsorption mechanism

The removal mechanisms of Cd by BC, CT-BC, and TH@CT-BC from contaminated solution were further investigated with SEM, EDS, FTIR, XRD (Figure 5), and XPS (Figure 2) analytical techniques. SEM images evidently showed the structural changes in BC, CT-BC, and TH@CT-BC after Cd adsorption, indicating the Cd deposition onto the porous adsorption sites of pristine and modified BCs. Similarly, EDS microanalysis (Figure 5) demonstrated an increment in Cd contents of CT-BC and TH@CT-BC after metal adsorption by 2.37 and 17.70%, implying that Cd was adsorbed onto the modified BC. These findings are consistent with the results of FTIR which indicated that surface complexation was the more prominent mechanism in Cd adsorption by CT-BC and TH@CT-BC.

As shown in Figure 5, no considerable change in the type of functional groups was observed after Cd adsorption onto TH@CT-BC which depicted that material maintained its structure even after the reaction. However, several peaks at 1241 (C─OH), 1412 (C─O and benzene ring), 1629 (C═C), and 3422 (O–H or N–H group) cm^{-1} were weakened which might be linked to the surface complexation and exchange of ligands between oxygenic functional groups and Cd. Similarly, shift in the peak of N–H band after Cd adsorption could be attributed between the interaction of amine functional groups of CT impregnated onto BC and Cd. Moreover, the decrease in band

intensity of these functional groups indicates the adsorption of Cd onto modified BC as reported in previous studies (Zhou et al., 2017; Zhou et al., 2018). It was worthy to note that a decrease in the peak intensity of the modified BC after Cd adsorption highlights the importance of thiol and amine groups for Cd (Zhang, Y et al., 2019). Thus, keeping these findings with the previous discussion, it can be expressed that surface functional groups were the dominant sites for surface complexation of Cd by TH@CT-BC.

The XRD analysis of BC, CT-BC, and TH@CT-BC after Cd adsorption is presented in Figure 5. After Cd adsorption, all the BCs showed new diffraction peaks indicating the formation of crystalline precipitates of cadmium cyanide and cadmium carbonate as dominant species in CT-BC while, cadmium carbonate, otavite, and silver cadmium in TH@CT-BC. Moreover, Cd adsorption yielded new diffraction peaks for all three BCs, which confirms the metal adsorption onto the BCs. The adsorption mechanism was further explored by using XPS analysis after Cd adsorption.

XPS spectra of BC, CT-BC (Figure S1), and TH@CT-BC (Figure 2) was recorded to further explore the Cd adsorption mechanisms onto pristine and modified BCs. The C1s and O1s spectra of TH@CT-BC showed the shifting in peaks after the Cd adsorption, where the C1s peaks at 284.05, 284.67, and 285.6 eV (C=C/C–C, C–O) were shifted to 283.89, 285.71, and 287.96 eV after Cd adsorption which mainly attributed to the involvement of oxygenic functional moieties in adsorption of Cd from contaminated solution. Similarly, the O1s peaks of TH@CT-BC corresponding to (O–H), (C=O), and (C–O) at 530.84, 531.69, and 532.79 eV shifted to 530.20, 531.12, and 532.05, respectively, indicating the oxygenic moieties as the preferential adsorption sites for Cd removal. After Cd adsorption, N1s peaks were disappeared for all the BCs while, new characteristic peaks of Cd e.g. Cd3d appeared in the XPS spectrum (Figure 2 and Figure S1). The

apparent peaks at 404.49, 405.42, 411.33, and 413.71 in TH@CT-BC indicate the adsorption of Cd. The doublet peaks around 404.49/405.42 and 411.33/413.71 might be associated to the Cd adsorption onto TH@CT-BC. Moreover, peaks around 411.4 ($Cd3d_{3/2}$) indicate the precipitation and complexation as the prevailing mechanisms for Cd adsorption e.g. cadmium hydroxide and carbon oxides (Huang et al., 2018), however, peak intensities at 404.6 eV ($Cd3d_{5/2}$) (Wu et al., 2017) specifies that Cd species were bind to thiol group via the binding reactions (Fan et al., 2020). More specifically, these results illustrate that oxygen and nitrogen group from hydroxyl, carboxyl, and amine groups are the major active sites for Cd adsorption which were in line with the results of FTIR and XRD confirming the selective adsorption of Cd onto TH@CT-BC.

On the basis of all these findings, potential Cd adsorption mechanisms onto TH@CT-BC are illustrated in Figure 6. From, SEM, EDS, FTIR, XRD, and XPS analysis, it can be corroborated that oxygenic functional moieties played a considerable role in Cd adsorption onto TH@CT-BC. Moreover, surface complexation and active functional groups played key roles in metal-ligand interactions. In addition, electrostatic interactions can also partially contribute to Cd removal. So, it can be stated that a complex of BC, CT, and further TH modification yielded hydroxyl functional groups that contributed in an efficient removal of Cd via surface complexation and electrostatic interaction.

3.6. Regeneration of BC, CT-BC, and TH@CT-BC for Cd

The reusability of BC, CT-BC, and TH@CT-BC for the adsorptive removal of Cd was tested over 5 cycles and results are presented in Figure S4A. The adsorption capacity of BC for Cd decreased significantly from the first to the second cycle, which might be attributed to the part of Cd which remains un-desorbed on BC by occupying the adsorption sites. However, CT-BC only showed a

small variation in adsorption capacity across all 5 cycles. There was a slight decrease in adsorption ability of TH@CT-BC after 5 adsorption cycles but still remained higher (93%) than other adsorbents. This higher adsorption capacity of TH@CT-BC may be attributed to the excessive functional groups available after CT and TH modification which helps in complexing the Cd from contaminated solution. TH@CT-BC showed higher reusability and effective adsorption of Cd even after 5 cycles, implying it as an efficient adsorbent for metal recycling and wastewater purification.

3.7. Application of BC, CT-BC, and TH@CT-BC for Cd removal from spiked river water

The efficiency of BC, CT-BC, and TH@CT-BC for Cd removal from river water was evaluated by conducting the adsorption experiments in river water spiked with Cd (10 and 30 mg L^{-1}) (Figure S4B). Generally, multiple co-existing ions are present in the river water matrix that competes for the active adsorption sites onto the adsorbents. In this study, real river water was spiked with 10 and 30 mg L^{-1} Cd solution and treated with BC, CT-BC, and TH@CT-BC for Cd adsorption. Our results revealed that Cd removal efficiency of TH@CT-BC was slightly affected with an increase in metal concentration in the solution. In this study, highest removal efficiency was achieved with TH@CT-BC (93.22 and 88.55%) for Cd concentration of 10 and 30 mg L^{-1}. This greater removal efficiency might be attributed to the excellent adsorption characteristics of TH@CT-BC, indicating its fast adsorption rate, highest adsorption capacity, and suitability in wide pH range which make it feasible for metals removal from river water (Zhang et al., 2016).

4. Conclusions

This study demonstrated the production of highly effective rice straw biochar coated with chitosan and further grafted with thiol (3-mercaptopropyltrimethoxysilane). The pristine and modified BCs

were characterized using SEM, EDS, FTIR, XRD, and XPS techniques and characterization data reported a considerable effect on surface morphology of BC after modification. XPS results showed a change in oxygen contents in CT-BC and TH@CT-BC (26.42 and 32.86%) as compared to BC which had 15.54% oxygen contents. The batch adsorption results indicated that sorption capacity of TH@CT-BC for Cd (261.47 mg g^{-1}) was higher than CT-BC and BC (103.14 and 29.64 mg g^{-1}), respectively. Despite the presence of competing cations (Ni, Zn, Pb, Mg, and Cu), TH@CT-BC demonstrated highly selective adsorption of Cd (82.54, 82.01, 81.18, 81.06, and 79.11 mg g^{-1}). Moreover, it also displayed higher regeneration ability of around 93% indicates the remarkable performance of TH@CT-BC for Cd removal. The adsorption mechanisms were discussed and surface complexation through hydroxyl, carboxyl, and amine groups and electrostatic interactions appeared to be the major mechanisms of Cd removal from contaminated water. Finally, Cd removal from river water spiked with different doses of metal depicted a higher potential of TH@CT-BC for Cd recovery. Based on the easy synthesis, high adsorption efficiency, and environment-friendly nature, it can be pointed out that TH@CT-BC can be upscaled to remove Cd in real aqueous systems.

Acknowledgments

This research was funded by National Natural Science Foundation of China (#41721001; #31872956), Zhejiang Science and Technology Bureau, China (#2018C02029), the Fundamental Research Funds for the Central Universities, China, and Pioneer project of Zhejiang Science and Technology Plan (#2023C02002).

Declaration of competing interest

The authors declare they have no known competing financial interests or personal relationships that could influence the work reported in this paper.

Data availability

Data will be made available on request.

References

Abd Malek, N. N., Jawad, A. H., Ismail, K., Razuan, R., ALOthman, Z. A., 2021. Fly ash modified magnetic chitosan-polyvinyl alcohol blend for reactive orange 16 dye removal: Adsorption parametric optimization. Internat. J. Biologic. Macromolec. 189, 464–476.

Ahmed, M. B., Zhou, J. L., Ngo, H. H., Guo, W., Chen, M., 2016. Progress in the preparation and application of modified biochar for improved contaminant removal from water and wastewater. Bioresour. Technol. 214, 836–851.

Bahrudin, N. N., Nawi, M. A., Jawad, A. H., Sabar, S., 2020. Adsorption Characteristics and Mechanistic Study of Immobilized Chitosan-Montmorillonite Composite for Methyl Orange removal. J. Polymers Environ. 28, 1901–1913.

Chai, L., Li, Q., Zhu, Y., et al., 2010. Synthesis of thiol-functionalized spent grain as a novel adsorbent for divalent metal ions. Bioresour. Technol. 101 (15), 6269–6272.

Chen, X., Chen, G., Chen, L., Chen, Y., Lehmann, J., McBride, M. B., Hay, A. G., 2011. Adsorption of copper and zinc by biochars produced from pyrolysis of hardwood and corn straw in aqueous solution. Biores. Technol. 102, 8877–8884.

Deng, S., Wang, P., Zhang, G., Dou, Y., 2016. Polyacrylonitrile-based fiber modified with thiosemicarbazide by microwave irradiation and its adsorption behavior for Cd (II) and Pb (II). J. Hazard. Mater. 307, 64–72.

Deng, Y., Li, X., Ni, F., Liu, Q., Yang, Y., Wang, M., Ao, T., Chen, W., 2021. Synthesis of Magnesium Modified Biochar for Removing Copper, Lead and Cadmium in Single and Binary Systems from Aqueous Solutions: Adsorption Mechanism. Water 13, 599.

Fan, J., Cai, C., Chi, H., Reid, B.J., Coulon, F., Zhang, Y., Hou, Y., 2020. Remediation of cadmium and lead polluted soil using thiol-modified biochar. J. Hazard. Mater. 388, 122037.

Fan, L. L., Luo, C. N., Sun, M., Li, X.J., Qiu, H.M., 2013. Highly selective adsorption of lead ions by water-dispersible magnetic chitosan/graphene oxide composites, Colloid. Surf. B 103 523–529.

Freundlich, H., 1906. Over the adsorption in solution, Z. Phys. Chem. 385–470 (1906).

Hamid, Y., Liu, L., Usman, M., Naidu, R., Hussain, M. I., Yang, X., 2022. Functionalized biochars: synthesis, characterization, and application for the removal of potentially harmful elements from water. J. Hazard. Mat. 437, 129337.

Haris, M., Usman, M., Su, F., Lei, W., Saleem, A., Hamid, Y., Guo, J., Li, Y., 2022. Programmable synthesis of exfoliated biochar nanosheets for selective and highly efficient adsorption of thallium. Chem. Eng. J. 434, 134842.

He, F., Wang, W., Moon, J. W., Howe, J., Pierce, E. M., Liang, L., 2012. Rapid removal of Hg(II) from aqueous solutions using thiol-functionalized Zn-doped biomagnetite particles, ACS Appl. Mater. Interfaces 4, 4373–4379.

Huang, Y., Tang, J., Gai, L., Gong, Y., Guan, H., He, R., Lyu, H., 2017. Different approaches for preparing a novel thiol-functionalized graphene oxide/Fe-Mn and its application for aqueous methylmercury removal. Chem. Eng. J. 319, 229–239.

Huang, Y., Xia, S., Lyu, J., Tang, J., 2019a. Highly efficient removal of aqueous Hg^{2+} and CH_3Hg^+ by selective modification of biochar with 3 mercaptopropyltrimethoxysilane. Chem. Eng. J. 360,1646–1655.

Huang, Y., Zhao, W., Zhang, X., Peng, H., Gong, Y., 2019b. Thiol-ene synthesis of thioether/ carboxyl-functionalized polymers for selective adsorption of silver (I) ions, Chem. Eng. J. 375, 121935.

Inyang, M. I., Gao, B., Yao, Y., Xue, Y., Zimmerman, A., Mosa, A., Pullammanappallil, P., Ok, Y. S., Cao, X., 2016. A review of biochar as a low-cost adsorbent for aqueous heavy metal removal, Crit. Rev. Environ. Sci. Technol. 46, 406–433.

Jawad, A. H., Abdulhameed, A. S., Surip, S. N., Sabar, S., 2022. Adsorptive performance of carbon modified chitosan biopolymer for cationic dye removal: kinetic, isotherm, thermodynamic, and mechanism study. Internat. J. Environ. Analytic. Chem. 18, 6189–6203.

Jawad, A. H., Abdulhameed, A. S., Wilson, L. D., Hanafiah, M. A. K. M. Nawawi, W. I., ALOthman, Z. A., Khan, M. R., 2021. Fabrication of Schiff's Base Chitosan-Glutaraldehyde/Activated Charcoal Composite for Cationic Dye Removal: Optimization Using Response Surface Methodology. J. Polymers Environ. 29, 2855–2868.

Jiang, L., Li, S., Yu, H., et al., 2016. Amino and thiol modified magnetic multi-walled carbon nanotubes for the simultaneous removal of lead, zinc, and phenol from aqueous solutions. Appl. Surf. Sci. 369, 398–413.

Karunanayake, A.G., Todd, O.A., Crowley, M., Ricchetti, L., Pittman Jr., C.U., Anderson, R., Mohan, D., Mlsna, T., 2018. Lead and cadmium remediation using magnetized and nonmagnetized biochar from Douglas fir. Chem. Eng. J. 331, 480–491.

Kazemi, F., Younesi, H., Ghoreyshi, A. A., Bahramifar, N., Heidari, A., 2016. Thiol-incorporated activated carbon derived from fir wood sawdust as an efficient adsorbent for the removal of mercury ion: batch and fixed-bed column studies, Process Saf. Environ. Prot. 100, 22–35.

Krasucka, P., Pan, B., Ok, Y. S., Mohan, D., Sarkar, B., Oleszczuk, P., 2021. Engineered biochar – A sustainable solution for the removal of antibiotics from water. Chem. Eng. J. 405, 126926.

Langmuir, I., 1917. The constitution and fundamental properties of solids and liquids, II. Liquids. J. Am. Chem. Soc. 39, 1848–1906.

Lima, E. C., Adebayo, M.A., 2015. Kinetic and Equilibrium Models of Adsorption, © Springer International Publishing Switzerland. https://doi.org/10.1007/ 978-3-319-18875-1.

Liu, X., Sun, J., Xu, X., Alsaedi, A., Hayat, T., Li, J., 2019. Adsorption and desorption of U(VI) on different-size graphene oxide, Chem. Eng. J. 360, 941–950.

Ma, J. H., Luo, J. M., Liu, Y. T., Wei, Y. F., Cai, T., Yu, X. W., Liu, H., Liu, C. B., Crittenden, J. C., 2018. Pb(II), Cu(II) and Cd(II) removal using a humic substance-based double network hydrogel in individual and multicomponent systems, J. Mater. Chem. A 6, 20110–20120.

Mohan, D., Pittman, C. U. Jr., Bricka, M., Smith, F., Yancey, B., Mohammad, J., Steele, P. H., Alexandre-Franco, M. F., G omez-Serrano, V., Gong, H., 2007. Sorption of arsenic, cadmium, and lead by chars produced from fast pyrolysis of wood and bark during bio-oil production. J. Colloid Interface Sci. 310, 57–73.

Mohan, D., Sarswat, A., Ok, Y. S., Pittman, C. U., 2014. Organic and inorganic contaminants removal from water with biochar, a renewable, low cost and sustainable adsorbent – a critical review, Bioresour. Technol. 160, 191–202.

Pehlivan, E., Yanik, B.H., Ahmetli, G., et al., 2008. Equilibrium isotherm studies for the uptake of cadmium and lead ions onto sugar beet pulp. Bioresour. Technol. 99 (9), 3520–3527. https://doi.org/10.1016/j.biortech.2007.07.052.

Penido, E.S., Melo, L.C.A., Guilherme, L.R.G., Bianchi, M.L., 2019. Cadmium binding mechanisms and adsorption capacity by novel phosphorus/magnesium-engineered biochars. Sci. Total Environ. 671, 1134–1143.

Qi, F., Dong, Z., Naidu, R., Bolan, N.S., Lamb, D., Yong, S.O., Liu, C., Khan, N., Johir, M. A. H., Semple, K. T., 2017. Effects of acidic and neutral biochars on properties and cadmium retention of soils. Chemosph. 180, 564–573.

Sackey, E. A., Song, Y., Yu, Y., Zhuang, H., 2021. Biochars derived from bamboo and rice straw for sorption of basic red dyes. PLoS ONE 16(7): e0254637.

She, H., Ma, X., Chang, G., 2018. Highly efficient and selective removal of N-heterocyclic aromatic contaminants from liquid fuels in a Ag(I) functionalized metal-organic framework: contribution of multiple interaction sites, J. Colloid. Interface Sci. 518, 149–155.

Son, E.B., Poo, K.M., Chang, J.S., Chae, K.J., 2017. Heavy metal removal from aqueous solutions using engineered magnetic biochars derived from waste marine macroalgal biomass. Sci. Total Environ. 615, 161–168.

Tan, X., Wei, W., Xu, C., Meng, Y., Bai, W., Yang, W., Lin, A., 2020. Manganese-modified biochar for highly efficient sorption of cadmium. Environ. Sci. Pollut. Res. 27, 9126–9134.

Tang, J., Huang, Y., Gong, Y., Lyu, H., Wang, Q., Ma, J., 2016. Preparation of a novel graphene oxide/Fe-Mn composite and its application for aqueous Hg(II) removal, J. Hazard. Mater. 316, 151–158.

Turan, V., 2019. Confident performance of chitosan and pistachio shell biochar on reducing Ni bioavailability in soil and plant plus improved the soil enzymatic activities, antioxidant defense system and nutritional quality of lettuce. Ecotoxicol. Environ. Saf. 183, 109594.

Wan, M.W., Kan, C.C., Rogel, B.D., Dalida, M.L.P., 2010. Adsorption of copper (II) and lead (II) ions from aqueous solution on chitosan-coated sand, Carbohyd. Polym. 80, 891–899.

Wan, X., Li, C., Parikh, S. J., 2020. Simultaneous removal of arsenic, cadmium, and lead from soil by iron-modified magnetic biochar. Environ. Pollut. 261, 114157.

Wang, R., He, Z., Wang, W., Bu, J., Wang, D., Zeng, G., Zhou, C., Xiong, W., Yang, Y., 2023. Rational design of cobalt sulfide anchored on nitrogen-doped carbon derived from *cyanobacteria* waste enables efficient activation of peroxymonosulfate for organic pollutants oxidation. Chemosph. 314, 137733.

Wang, S., Yu, D.M., 2010. Adsorption of Cd(II), Pb(II), and Ag(I) in aqueous solution on hollow chitosan microspheres, J. Appl. Polym. Sci. 118, 733–739.

Wu, A., Tian, C., Jiao, Y., Yan, Q., Yang, G., Fu, H., 2017. Sequential two-step hydrothermal growth of MoS2 /CdS core-shell heterojunctions for efficient visible light-driven photocatalytic H_2 evolution. Appl. Catal. B Environ. 203, 955–963.

Wu, J., Huang, D., Liu, X., Meng, J., Tang, C., Xu, J., 2018b. Remediation of As(III) and Cd(II) co-contamination and its mechanism in aqueous systems by a novel calciumbased magnetic biochar. J. Hazard. Mat. 348, 10–19.

Xia, S., Huang, Y., Tang, J., Wang, L., 2019. Preparation of various thiol-functionalized carbon-based materials for enhanced removal of mercury from aqueous solution. Environ. Sci. Pollut. Res. https://doi.org/10.1007/s11356-019-04320-0.

Xia, W., Song, B., Yi, H., Almatrafi, E., Yang, Y., Fu, Y., Huo, X., Qin, F., Xiang, L., Zeng, Y., Zeng, G., Zhou, C., 2022. From aquatic biota to autogenous N-doping biochar—using a highly efficient nonradical dominant process for sulfamethoxazole degradation. J. Clean. Produc. 373, 133750.

Xiao, L. L., Wang, N., Ping, N. A., 2013. Preparation and properties of thiolfunctionalized activated carbon for selective removal of mercury(II) ions. Mod. Chem. Ind. 10, 70–75.

Xie, Y., Huang, W., Zheng, B., Li, S., Liu, Q., Chen, Z., Mai, W., Fu, R., Wu, D., 2019. All-in-one porous polymer adsorbents with excellent environmental chemosensory responsivity, visual detectivity, superfast adsorption, and easy regeneration, Adv. Mater 31 (16), 1900104.

Xu, Z., Hu, Y., Guo, Z., Xiao, X., Peng, C., Zeng, P., 2022. Optimizing pyrolysis temperature of contaminated rice straw biochar: Heavy metal(loid) deportment, properties evolution, and Pb adsorption/ immobilization. J. Saudi Chem. Soc. 26, 101439.

Xue, Y., Gao, B., Yao, Y., Inyang, M., Zhang, M., Zimmerman, A. R., Ro, K. S., 2012. Hydrogen peroxide modification enhances the ability of biochar (hydrochar) produced from hydrothermal carbonization of peanut hull to remove aqueous heavy metals: batch and column tests, Chem. Eng. J. 200, 673–680.

Zhang, G., Fan, F., Li, X., Qi, J., Chen, Y., 2018. Superior adsorption of thallium(I) on titanium peroxide : Performance and mechanism, Chem. Eng. J. 331, 471–479.

Zhang, L., Tang, S., He, F., Liu, Y., Mao, W., Guan, Y., 2019. Highly efficient and selective capture of heavy metals by poly(acrylic acid) grafted chitosan and biochar composite for wastewater treatment. Chem. Eng. J. 378, 122215.

Zhang, X., Qian, J., Pan, B., 2016. Fabrication of novel magnetic nanoparticles of multifunctionality for water decontamination, Environ. Sci. Tec hnol. 50 (2), 881–889.

Zhang, Y., Yue, X., Xu, W., Zhang, H., Li, F., 2019. Amino modification of rice straw-derived biochar for enhancing its cadmium (II) ions adsorption from water. J. Hazard. Mat. 379, 120783.

Zhou, L., Huang, Y., Qiu, W., Sun, Z., Liu, Z., Song, Z., 2017. Adsorption properties of nanoMnO_2–biochar composites for copper in aqueous solution. Molecules 22, 173–186.

Zhou, Q., Liao, B., Lin, L., Qiu, W., Song, Z., 2018. Adsorption of Cu(II) and Cd(II) from aqueous solutions by ferromanganese binary oxide–biochar composites. Sci. Total Environ. 615, 115–122.

Zhou, Y. M., Gao, B., Zimmerman, A.R., Fang, J. E., Sun, Y. N., Cao, X. D., 2013. Sorption of heavy metals on chitosan-modified biochars and its biological effects, Chem. Eng. J. 231, 512–518.

Table 1: Various properties of pristine and modified biochars

Biochar	N[a]	C[a]	H[a]	C/N ratio	H/C	pH	Surface area (m^2/g)	C%[b]	O%[b]	N%[b]
BC	1.23	49.64	2.26	40.35	0.04	9.07	12.36	81.67	15.54	2.40
CT-BC	2.27	38.35	3.97	16.89	0.10	9.14	4.87	69.66	26.42	3.62
TH@CT-BC	0.75	33.09	4.90	44.12	0.14	8.81	3.59	65.44	32.84	1.34

a: data from elemental analyser

b: data from XPS results presenting the atomic percentage of elements

Here, BC: rice straw biochar, CT-BC: chitosan-modified rice straw biochar, and TH@CT-BC: thiol grafted chitosan-modified biochar

Table 2: Isotherm parameters for Cd adsorption on BC, CT-BC, and TH@CT-BC

	Langmuir model	Freundlich model	Temkin model

	Q_{max} (mg g^{-1})	k_L(L mg^{-1})	R^2	K_F (L g^{-1})	1/n	R^2	k_T (L g^{-1})	b (KJ mol^{-1})	R^2
BC	29.64	0.0044	0.993	9.55	0.976	0.958	0.1176	0.932	9.337
CT-BC	103.14	0.0829	0.976	25.93	0.259	0.938	0.1389	0.768	33.672
TH@CT-BC	261.47	0.1290	0.987	70.06	0.618	0.949	8.8020	0.925	53.937

Here, BC: rice straw biochar, CT-BC: chitosan-modified rice straw biochar, and TH@CT-BC: thiol grafted chitosan-modified biochar

Table 3: Evaluation of adsorption capacity of Cd onto TH@CT-BC with other adsorbents

Adsorbent	Dosage (g/L)	Metal	Adsorption capacity (mg/g)	References
Amino modified rice straw biochar	0.1	Cd	74.6	Zhang, Y et al., 2019
Thiol modified rice straw biochar	0.025	Cd and Pb	45.1 and 61.4	Fan et al., 2020
Poly(acrylic acid) grafted chitosan and biochar composite	0.1	Cd and Pb	370.37 and 476.19	Zhang, L et al., 2019
Calcium-based magnetic biochar	0.05	Cd and As	10.07 and 6.34	Wu et al., 2018
Magnetic biochar	0.5	Cd, Cu, and Zn	23.16, 55.86, and 22.22	Son et al., 2017
Magnetic biochar from Douglas fir	0.01	Cd and Pb	18.50 and 64.80	Karunanayake et al., 2018
Manganese-modified biochar	0.025, 0.05, 0.1	Cd	191.94	Tan et al., 2020
Magnesium modified biochar	0.01	Cd, Cu, Pb	164.51, 200.33, and 448.50	Deng et al., 2021

Phosphorus/magnesium-engineered biochars	0.04	Cd	113.90	Penido et al., 2019
Rice straw biochar with thiol grafted chitosan composites	0.05	Cd	261.47	This study

Figure 1: SEM images, EDS spectra, FTIR peaks, and XRD spectral peaks of pristine and functional biochars

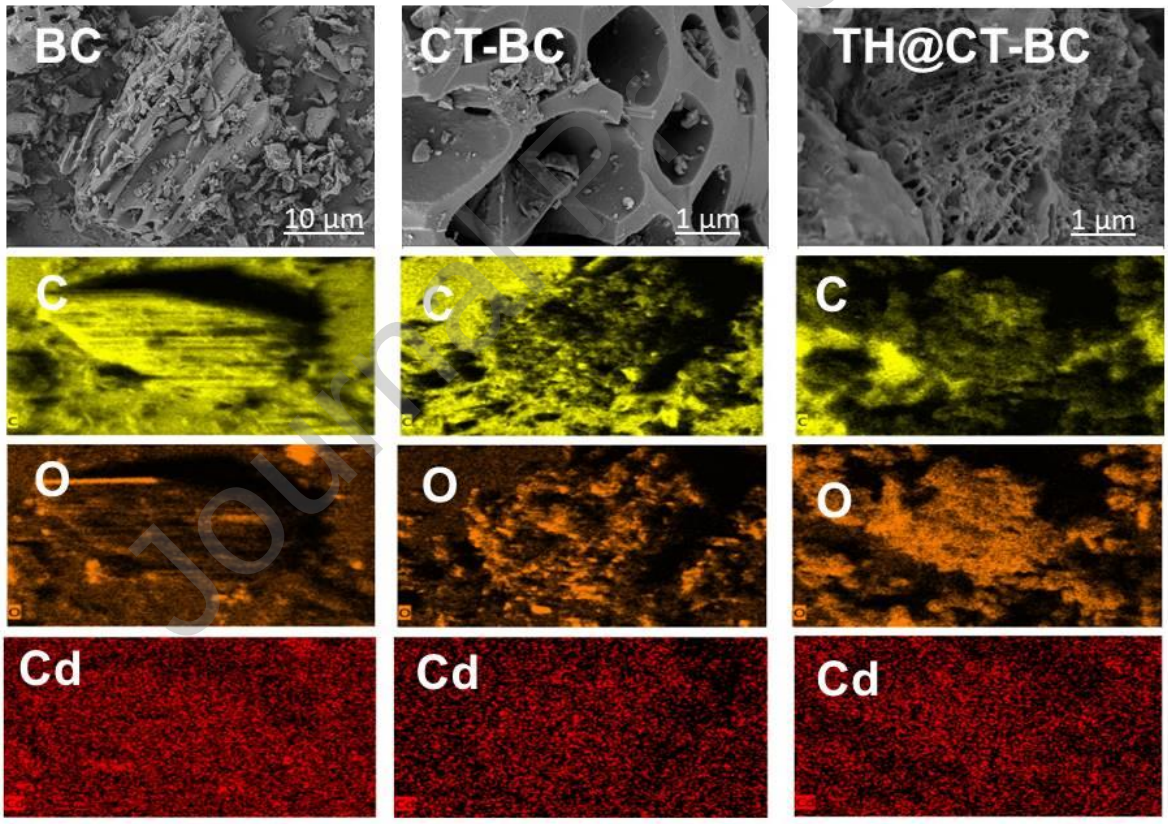

FTIR

XRD

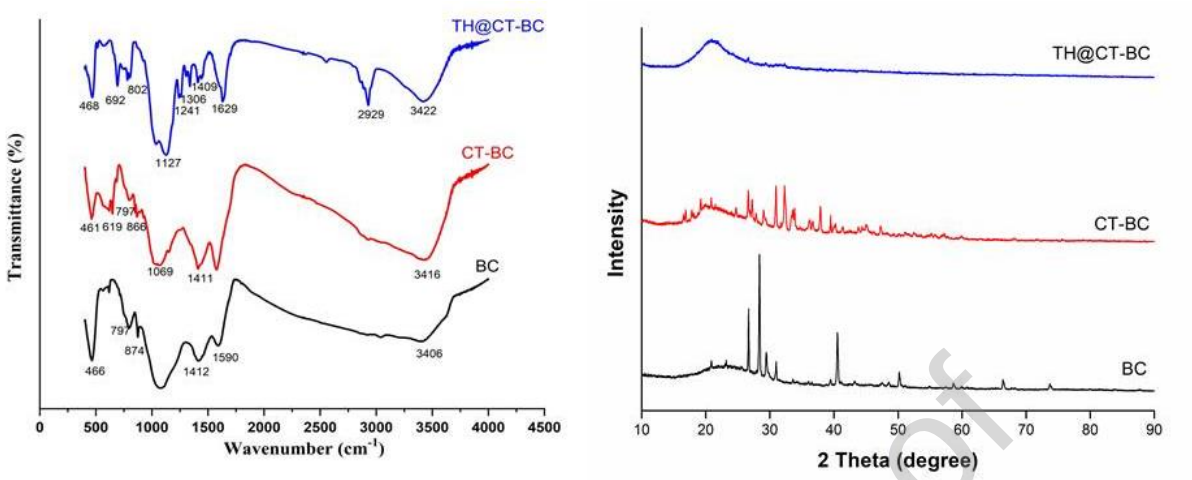

Figure 2: C1s, O1s, N1s, and Cd3d XPS spectra of TH@CT-BC before and after Cd adsorption

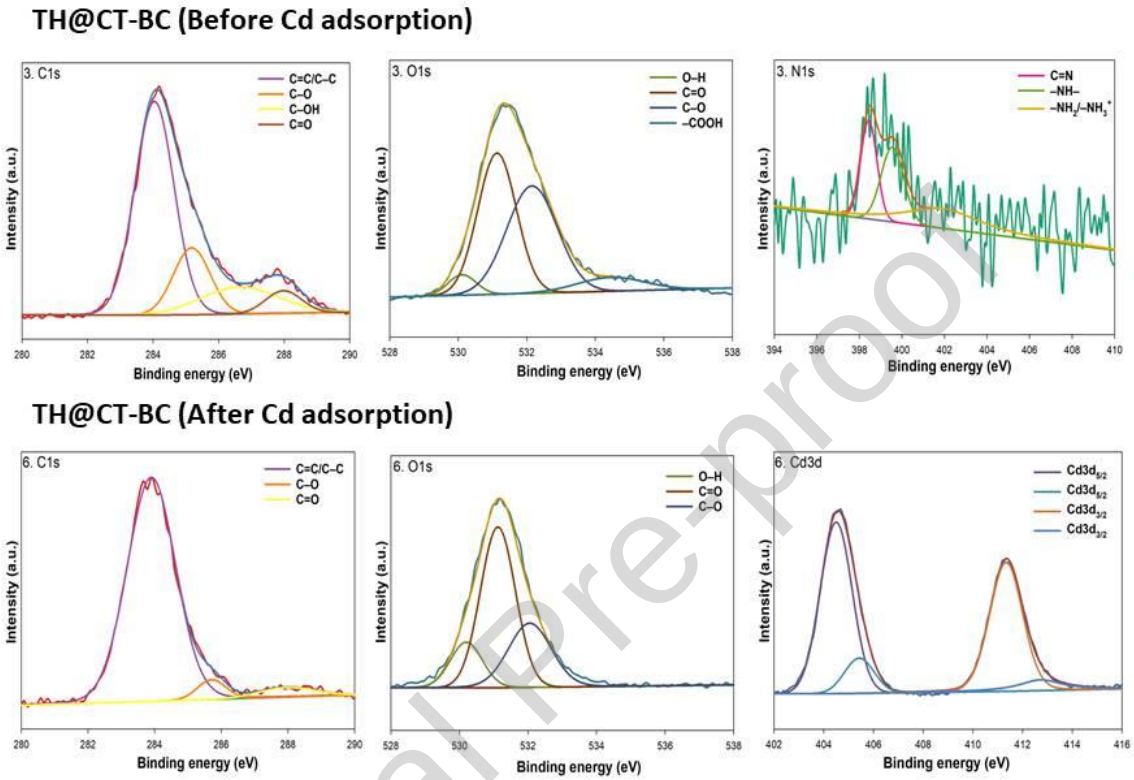

Figure 3: Kinetic adsorption of Cd onto BC, CT-BC, and TH@CT-BC and Pseudo-first order (straight line) and Pseudo-second order (straight line) curve fitting models (A), Intraparticle diffusion model (B). Reaction settings: Initial Cd concentration of 40 mg L^{-1}, adsorbent dosage 0.05 g, temperature 26±2 ºC, and pH 5.5±0.5

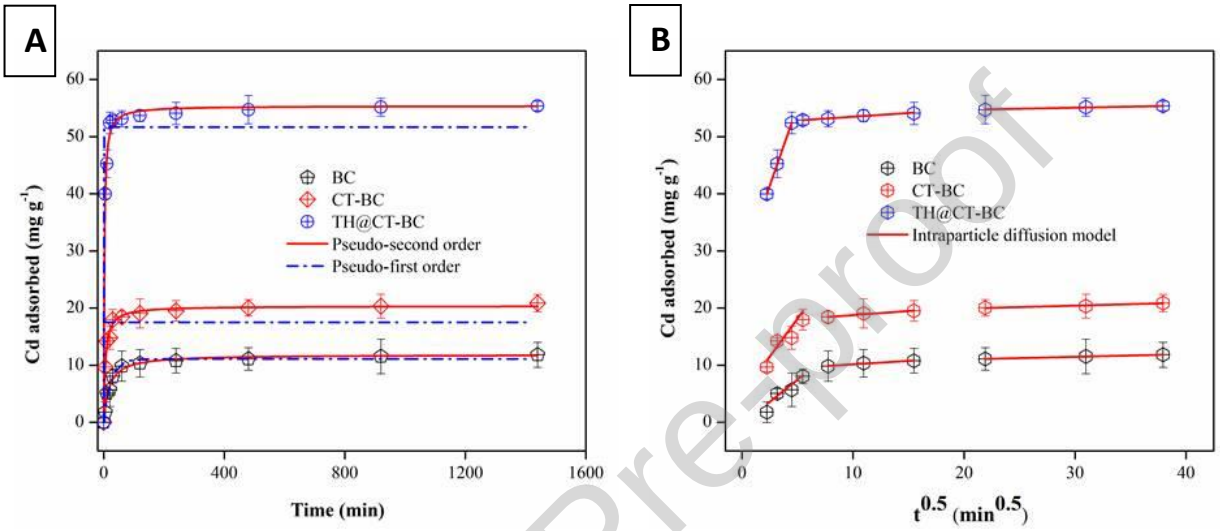

Figure 4: Sorption isotherms of Cd onto BC, CT-BC, and TH@CT-BC. Reaction settings: Adsorbent dosage 0.05 g, metal solution 35 mL, temperature 26±2 ºC, pH 5.5±0.5, and 200 rpm for 24 h.

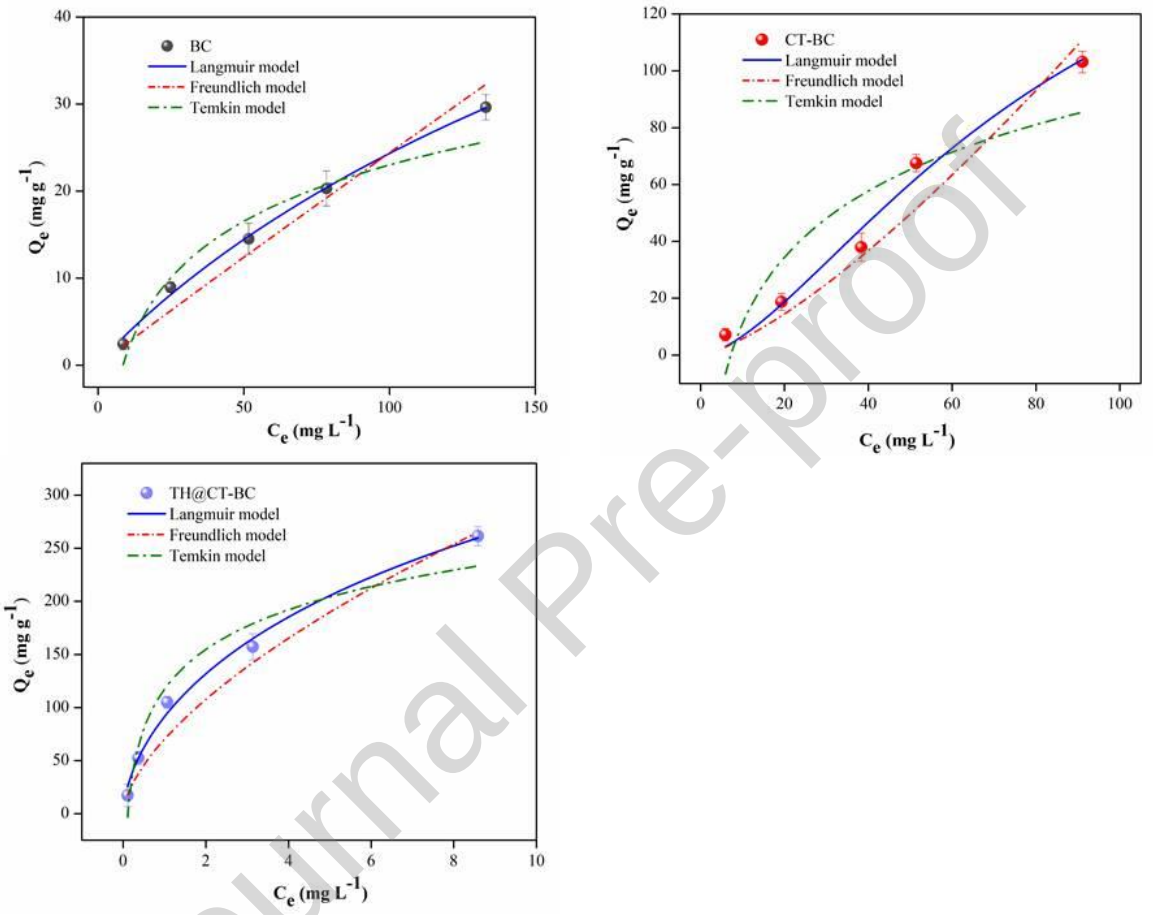

Figure 5: SEM images, EDS spectra, FTIR peaks, and XRD spectral peaks of pristine and functional biochars after Cd adsorption

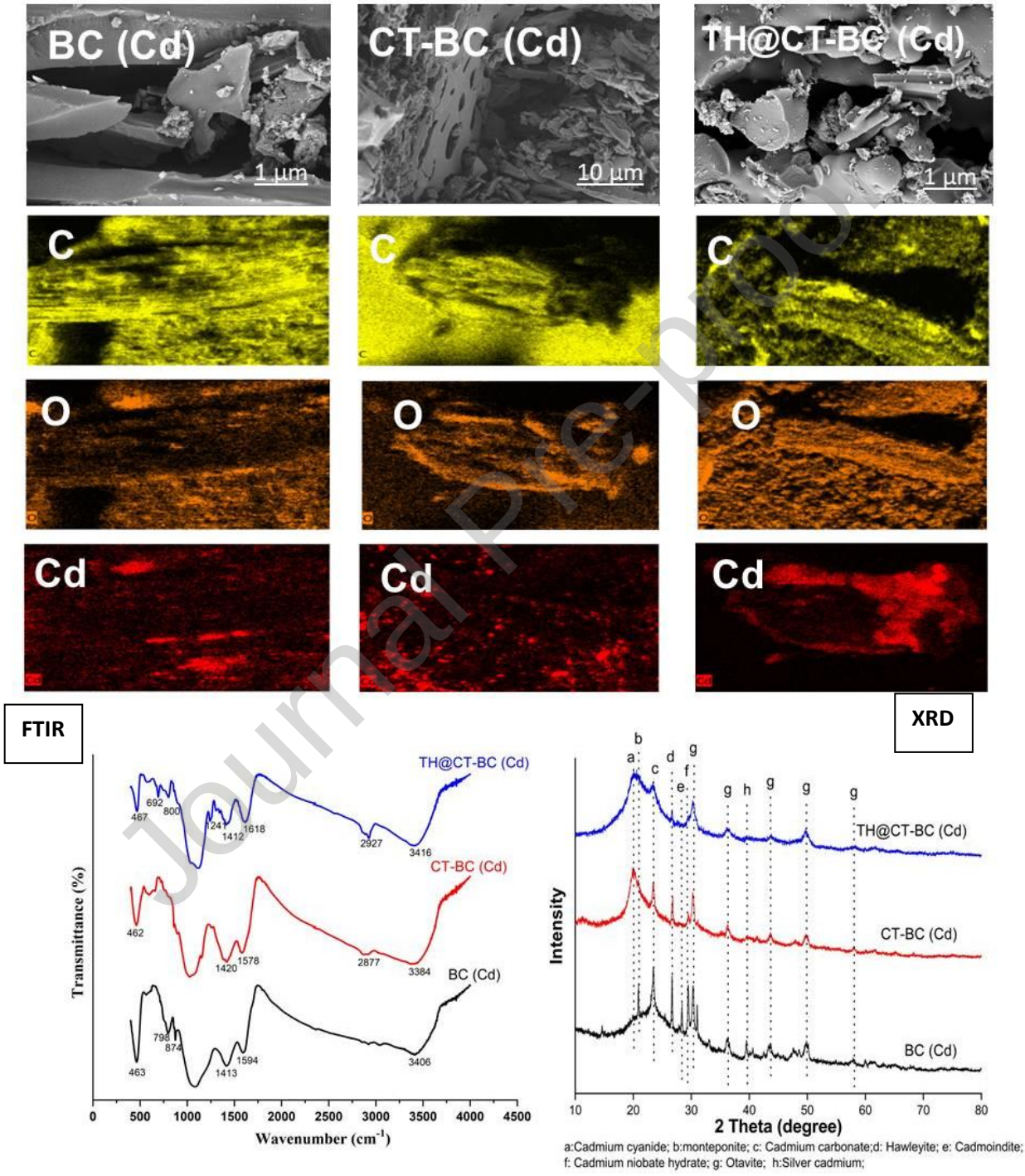

Figure 6: Schematic illustration of modification of rice straw biochar with 3 mercaptopropyltrimethoxysilane grafted chitosan composites (TH@CT-BC) (A) and potential mechanisms for Cd adsorption (B)

A

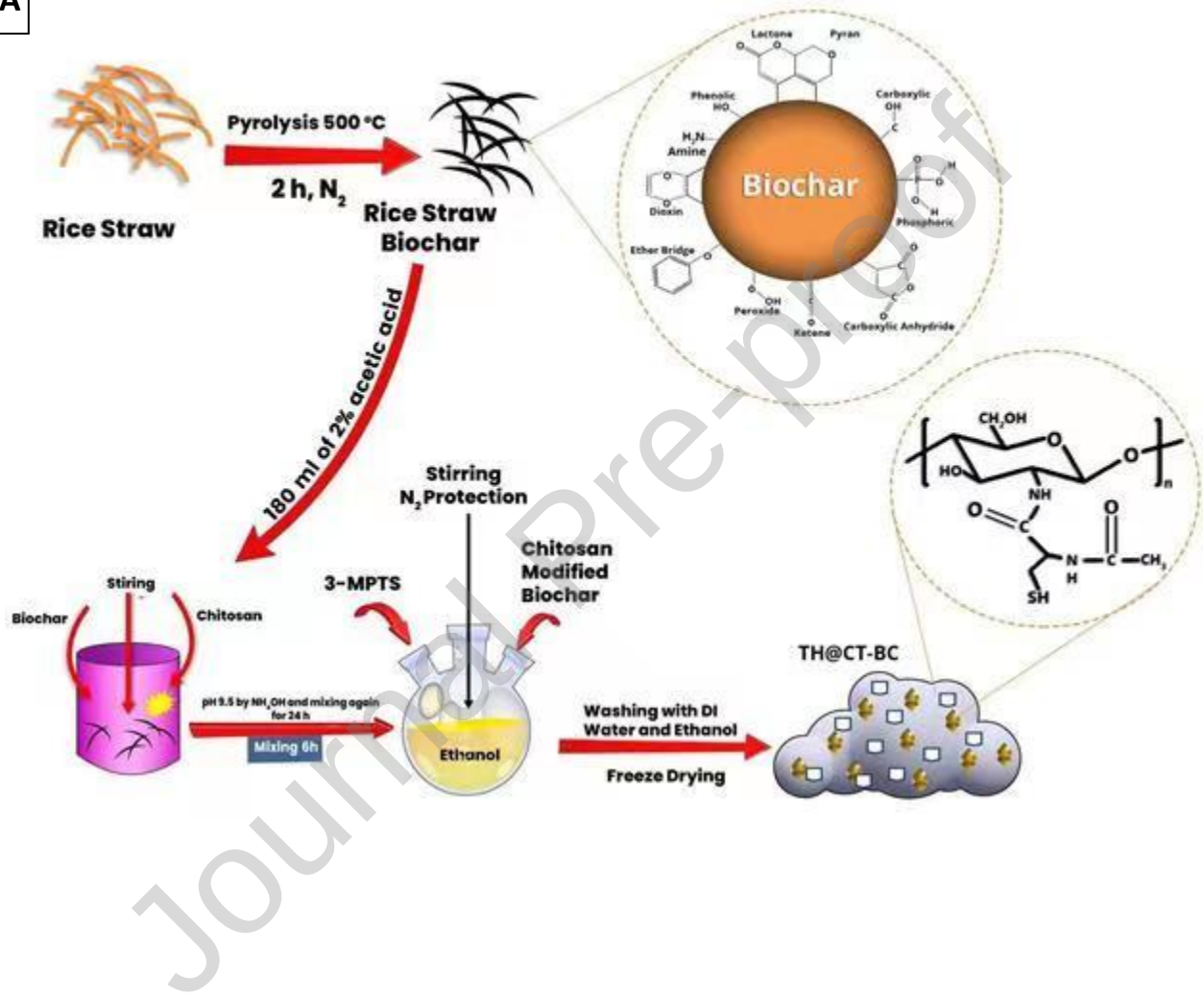

B

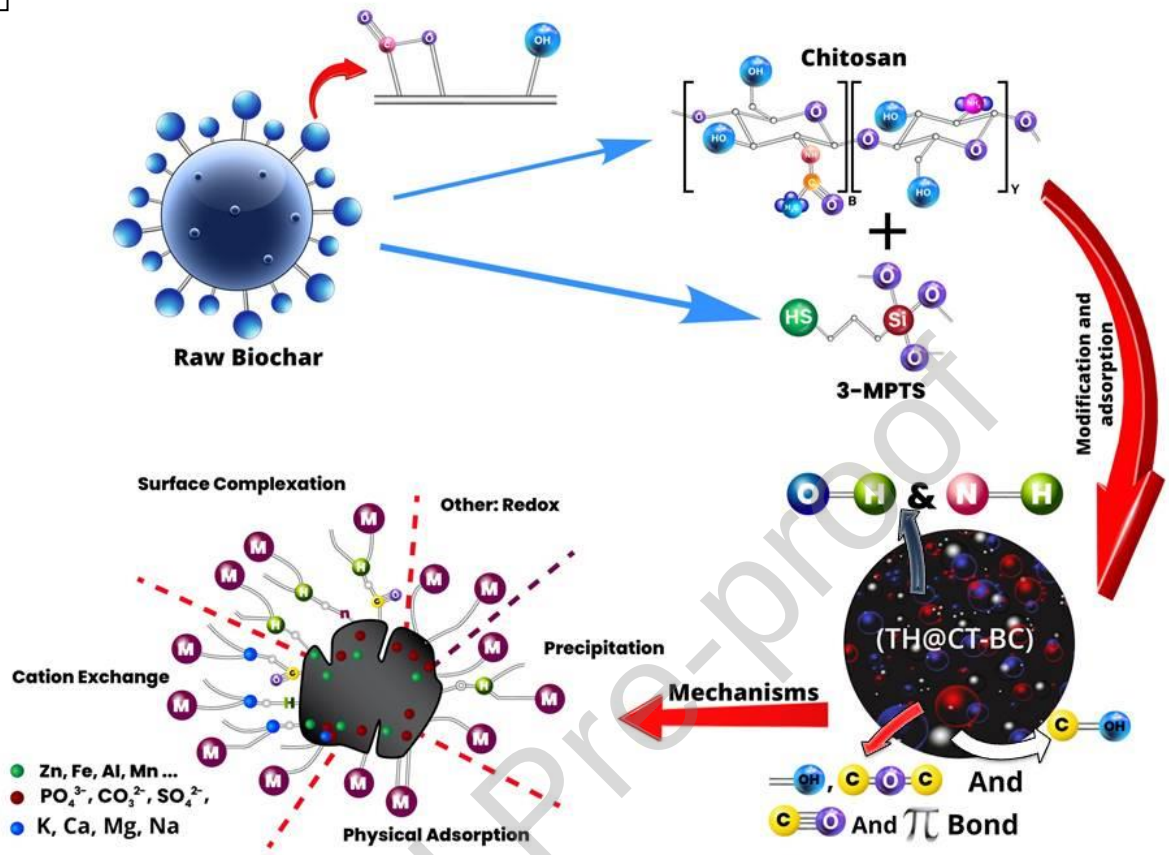

CRediT authorship contribution statement

Yasir Hamid: Methodology, Formal analysis, Original draft writing, Lei Liu: Formal analysis, Muhammad Haris: Conceptulization, Muhammad Usman: Reviewing and editing, Qiang Lin: Conceptualization, Yonglong Chen: Formal analysis, Muhammad Saqib Rashid: Formal analysis, Zaid Ulhassan: Reviewing and editing, M. Iftikhar Hussain: Reviewing and editing, Xiaoe Yang: Supervision

Declaration of interests

☐ √ The authors declare that they have no known competing financial interests or personal relationships that could have appeared to influence the work reported in this paper.

Highlights

- A two-step fabrication successfully loaded the thiol group onto chitosan-modified biochar
- Novel thiol-grafted composite of chitosan and rice straw biochar yielded in highly effective Cd adsorption
- Characterization of TH@CT-BC with FTIR, XRD, and XPS revealed the adsorption of Cd with imported functional moieties
- TH@CT-BC was established as a potential candidate for practical wastewater treatment applications